Effect of Montmorillonite on Orientation of Drawn Polypropylene Films

Bing Zhou, Yi-Liao Liu, Jun-Ting Xu, Zhi-Qiang Fan

MOE Key Laboratory of Macromolecular Synthesis and Functionalization, Department of Polymer Science and Engineering, Zhejiang University, Hangzhou 310027, China

Received 22 February 2011; accepted 23 May 2011
DOI 10.1002/app.34973
Published online 9 September 2011 in Wiley Online Library (wileyonlinelibrary.com).

ABSTRACT: Films of polypropylene/organically modified montmorillonite (PP/OMMT) nanocomposites were drawn at two different temperatures with various draw ratios. The effect of OMMT on the orientations of the crystalline and amorphous phases was studied using polarized infrared spectroscopy. It is found that OMMT layers always retard the orientation of the crystalline phase. The higher the OMMT loading, the stronger the retardance effect. In contrast, the effect of OMMT layers on the orientation of the amorphous phase depends on draw temperature and OMMT loading. A favorable effect on the orientation of the amorphous phase is observed at low OMMT loading and high draw temperature, but the retardance prevails at high OMMT loading and low draw temperature. The favorable effect on orientation at high draw temperature is attributed to the stabilization effect of OMMT layers on the conformation of amorphous PP chains. Such an effect was further verified by comparing the crystallization behavior and the morphologies of drawn PP and PP/OMMT films crystallized from 180°C. Memory effect is observed for crystallization of drawn PP/OMMT film, but it is not obvious for the drawn film of neat PP. Spherulites are formed for orientated neat PP films cooled from 180°C, but cylindrites are still formed after the drawn PP/OMMT films undergo melting at 180°C and recrystallization. The stabilization effect disappears at higher temperature (230°C). J Appl Polym Sci 123: 3321–3330, 2012

Key words: polypropylene; nanocomposite; orientation; crystallization; montmorillonite

INTRODUCTION

Polymer/montmorillonite (MMT) nanocomposites have received many research interests in the past two decades due to the improved mechanical, thermal, and permeation properties.[1–6] When the polymer is crystallizable, the montmorillonite can also affect the crystallization behavior and thus the morphology and mechanical properties of the nanocomposites. For example, the montmorillonite may exert a nucleation effect on polymer crystallization, leading to a faster crystallization rate and a smaller size of spherulite.[7–11] However, when polymer chains are intercalated into the galleries of the montmorillonite layers, the mobility of polymer chains is reduced and crystallization is retarded.[11–14] Moreover, the crystal structure in the nanocomposites may be altered due to the presence of montmorillonite.

Orientated semicrystalline polymer materials usually exhibit better mechanical properties in the stretched directions and are widely used. For semicrystalline polymer/montmorillonite nanocomposites, there are two methods to obtain the orientated materials. The first method, which is the most frequently used, involves shearing or stretching the melt of the nanocomposite followed by crystallization.[15–24] In this case, nanocomposites with orientated cylindrite or "shish-kebab" or even fibrous morphology are usually prepared.[24–27] It is found that shearing the melt of polymer/montmorillonite nanocomposites can greatly enhance the nucleation activity of the montmorillonite layers.[28] In poly(butylene terephthalate)/multiwalled carbon nanotubes (PBT/MWNT) nanocomposites, it is also found that shearing the melt can alter the crystallization kinetics of the nanocomposites, depending on the temperature and the concentration of MWNT.[29] After crystallization, the orientation degree of the polymer crystals also increases due to so-called shear amplification effect.[24,30] The second method to prepare the orientated semicrystalline polymer/montmorillonite nanocomposites is drawing the nanocomposites below the melting temperature of the polymer crystals.[31–37] It is reported that drawing the nanocomposites at

Correspondence to: J.-T. Xu (xujt@zju.edu.cn).
Contract grant sponsor: National Natural Science Foundation of China; contract grant number: 51073138.
Contract grant sponsor: National Basic Research Program of China (973 Program); contract grant number: 2011CB606005.
Contract grant sponsor: State Key Laboratory of Chemical Engineering; contract grant number: SKL-ChE-10D04.

crystallization state can lead to slipping and exfoliation of the montmorillonite layers.[34] A few authors also found that the nanofillers in the nanocomposites may inhibit the orientation of polymer crystals,[37,38] which is in contrast with the shear of nanocomposite melt. It should be noted that both the crystalline phase and amorphous phase can be orientated during tensile drawing,[39,40] but the effect of montmorillonite layers on the orientation of the amorphous phase in semicrystalline polymer/montmorillonite nanocomposites is rarely reported. The phenomenon of strain-induced crystallization is frequently observed when rubber is undergoing tensile drawing. It is reported that the presence of nanofiller in the rubber can promote strain-induced crystallization.[41,42]

In the present work, the polypropylene/organically modified montmorillonite (PP/OMMT) nanocomposite films were drawn at two different temperatures with various draw ratios, and the effect of OMMT on orientations of both the crystalline and amorphous phases were investigated with polarized infrared and optical microscopy.

EXPERIMENTAL

Materials

Polypropylene (Brand: T30s) with a melting index of 3.0 was provided by SINOPEC Zhongyuan Petrochemical Corp. (Zhengzhou, China) in the form of pellets. The weight-average molecular mass and the polydispersity of PP determined by gel permeation chromatograph (GPC) are 2.7×10^4 and 6.19, respectively. The compatibilizer polypropylene-*g*-maleic anhydride (PP-*g*-MA) (Brand: HIS-008) powder was purchased from Honsea Enterprise Co. (Guangzhou, China). The grafting ratio of MA is higher than 0.8%. The weight-average molecular mass and the polydispersity of PP-*g*-MA determined by GPC are 5.0×10^4 and 3.96, respectively. The OMMT nanoclay, Nanomer 1.44P, was purchased from Nonocor (Chicago, IL). The OMMT was prepared by the supplier through ion-exchanging Na^+ MMT with dimethyl, dehydrogenated tallow. PP, PP-*g*-MA, and OMMT were dried in vacuum for 2 days at 50°C before use.

Preparation of the PP/OMMT nanocomposites

Prescribed amount of PP, PP-*g*-MA, and OMMT were first dry mixed. The ratio of PP-*g*-MA to PP was kept constant, 10 wt %. The amount of OMMT is 0, 2, 4, and 6% relative to neat PP (PP-*g*-MA was not included) by weight, respectively. The mixture was fed into a twin-screw extruder to prepare the PP/OMMT nanocomposites by melt-blending. Different screw speeds were tested and better dispersion of OMMT was observed at 35 rpm. As a result, this screw speed was applied for all sample preparation. The barrel temperatures were kept at 165–200°C from hopper to die. The L/D ratio of the extruder was 25/1. After extrusion, the extruded samples were pelletized. The nanocomposites with different OMMT contents were denoted as PP-2, PP-4 and PP-6, where the last numbers correspond to the weight percentage of OMMT. The PP/PP-*g*-MA blend used for control experiment is designated as PP-0.

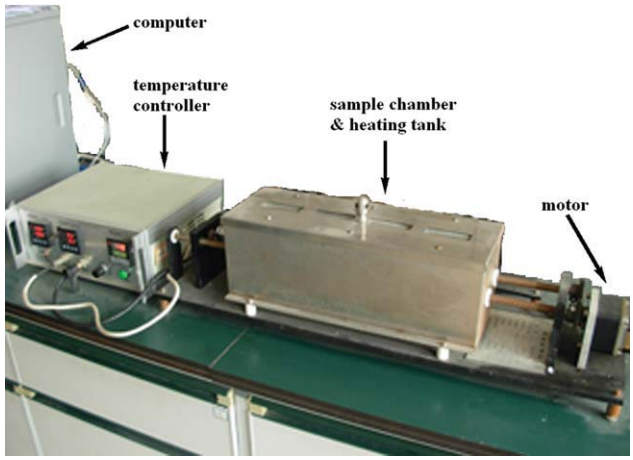

Figure 1 Picture of the tensile instrument. [Color figure can be viewed in the online issue, which is available at wileyonlinelibrary.com]

Tensile drawing

The PP/OMMT nanocomposites were first molded into films with a size of 20 mm (length) × 6 mm (width) by thermal compression. The nanocomposites were placed into the mold with the prescribed size and were kept at 220°C and 40 atm for 10 min, and then the compression machine was switched off and cooled to room temperature slowly. The films were drawn in a tensile instrument with a heating tank, which was designed by Beijing Kangsente Sci. and Tech. Co. The photo of the tensile instrument is shown in Figure 1. The samples were drawn at 110 and 138°C, respectively, with various draw ratios (λ). The draw rate was set as 1 mm/min. Before drawing, two lines were marked in the middle of the sample. The draw ratio was calculated from the ratio of the distances between these two lines after and before drawing. The areas near the center of the two marked lines in the drawn films were selected for FT-IR and optical microscopy characterizations. The thickness of the drawn films for FT-IR and optical microscopy characterizations was less than 80 μm.

Characterization

Morphology of the PP/OMMT nanocomposites was observed by transmission electron microscopy (TEM)

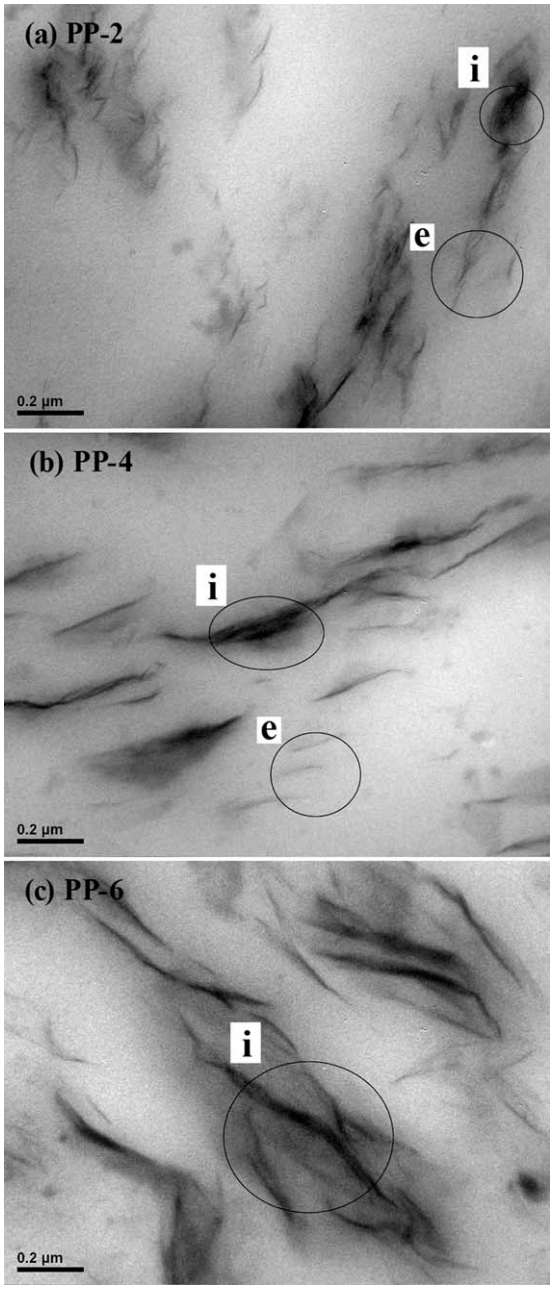

Figure 2 TEM images PP/OMMT nanocomposites. (a) PP-2, (b) PP-4, and (c) PP-6. In the images, the character "e" indicates the exfoliated OMMT layers and "i" indicates the intercalated OMMT layers.

on a JEOL JEM-1230 instrument (Tokyo, Japan) at an acceleration voltage of 80 kV. Room temperature wide angle X-ray diffraction (WAXD) experiments were carried out on a Rigaku Dmax/2550PC X-ray diffractometer (Tokyo, Japan) with X-ray wavelength $\lambda = 0.1542$ nm, operated at 40 kV and 30 mA. The range of diffraction angle for investigation was $2\theta = 2$–30° and the scanning step is 0.02°. Hot-press films were used for WAXD experiments. Differential scanning calorimetry (DSC) experiments were conducted on a TA Q200 instrument (New Castle, DE). The drawn films were cut into small pieces for DSC measurements. The sample weight was 3–5 mg and the samples were sealed in aluminum pans. The melting traces were recorded by heating the sample to 180°C at a rate of 10°C/min. For nonisothermal crystallization experiments, the drawn films were first held 180 or 230°C for 5 min, and then were cooled to room temperature at a rate of 10°C/min. An Olympus BX-5 (Tokyo, Japan) microscopy equipped with a hot-stage and a digital camera was used to observe the morphology of the drawn films. The drawn films were placed between two glass plates and heated to different temperatures (180 or 230°C) and held at these temperatures for 5 min. The morphology in the melt was recorded. Then the films were cooled to room temperature at a rate of 2°C/min and the morphology during nonisothermal crystallization was recorded. Polarized FT-IR experiments of the drawn films were carried out on a Nicolet 6700 spectrometer (Waltham, MA) with a transmission mode. The scan range was from 4000 to 400 cm^{-1} at an interval of 4 cm^{-1}. A polarizer was placed in front of the sample and the spectra at polarization angles of 0° (polarization vector parallel to the draw direction) and 90° (polarization vector perpendicular to the draw direction) were recorded for the same samples.

RESULTS AND DISCUSSION

Morphology of nanocomposites

After preparation of the PP/OMMT nanocomposites, the morphology of the bulk nanocomposites was first characterized to see the dispersion of the OMMT platelets. Figure 2 shows the TEM images of the nanocomposites. Both well-dispersed thin OMMT layers and aggregated OMMT layers can be observed for all the three PP/OMMT nanocomposites. This shows the coexistence of exfoliated and intercalated OMMT layers in the nanocomposites. One can also see that, with increase of the OMMT, the fraction of the intercalated OMMT layers increases. Figure 3 shows the WAXD patterns of the neat OMMT and PP/OMMT nanocomposites in the range of 2θ from 1° to 9°. As can be seen from Figure 3, the diffraction peak due to the stack of OMMT layers is very weak in PP-2 and PP-4, indicating that higher fraction of exfoliated OMMT layers are present in these two samples. The diffraction peak due to the stack of OMMT layers is strong for PP-6, but the position of this peak shifts to smaller angle as compared with the peak position of the neat OMMT. As a result, in PP-6 there exist lots of intercalated OMMT layers, which is in accordance with TEM observation.

Polarized FT-IR of the drawn films

When polarized FT-IR spectra with polarization vector both parallel and perpendicular to draw

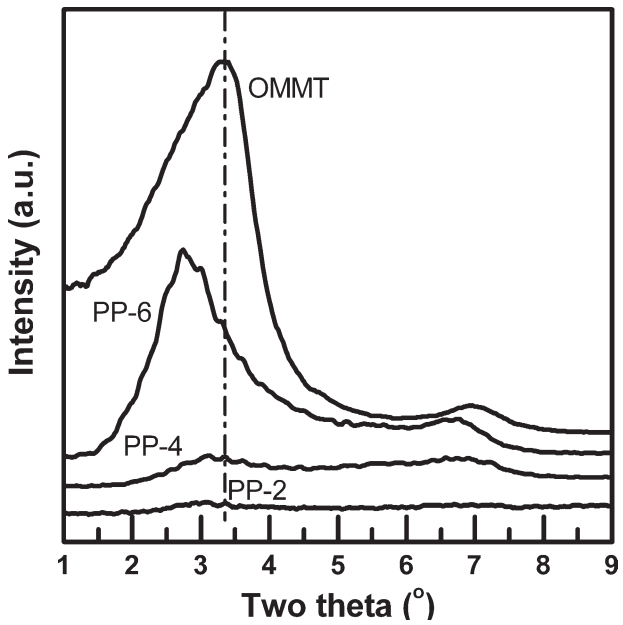

Figure 3 WAXD patterns of PP/OMMT nanocomposites and neat OMMT.

direction were obtained, the dichroic ratio (R) for a specific IR band can be calculated:

$$R = A_{||}/A_{\perp}, \tag{1}$$

where $A_{||}$ and $A_{\perp}$ are the integrated areas of the selected band parallel and perpendicular to draw direction, respectively.

The relationship between the Hermans orientation function (f) and dichroic ratio (R) can be expressed as[43]:

$$f = \frac{(R-1)(R_0+2)}{(R+2)(R_0-1)}, \tag{2}$$

where $R_0 = 2cot^2\phi$ and ϕ is the angle between the helix axis of polymer chains and IR transition moment.

Here we chose the bands at 841 and 2725 cm^{-1} for evaluation of orientation of the crystalline and amorphous phases, respectively.[43,44] The values of ϕ for the bands at 841 and 2725 cm^{-1} are 0° and 90°, respectively.[43–45] This means that the crystalline band at 841 cm^{-1} $A_{||}$ is larger than $A_{\perp}$ and the orientation degree increases with R of the crystalline band, while for the amorphous band at 2725 cm^{-1} $A_{||}$ is smaller than $A_{\perp}$ and the orientation degree increases with $1/R$ of the amorphous band, as exemplified in Figure 4.

We tried to plot f versus draw ratio. However, it is found that the difference in f between the PP-0 and PP/OMMT nanocomposites is not so evident, especially at higher draw ratios. This is in contrast with the larger difference of the IR spectra. In fact, one can see from the expression of the orientation function, f will minish the difference of R. At higher draw ratios, a large difference of R only leads to a slight change in f. As a result, we still use R (for the crystalline band) or $1/R$ (for the amorphous band) to plot against draw ratio. Figure 5 shows R of the crystalline band at 841 cm^{-1} and $1/R$ of the amorphous band at 2725 cm^{-1} for PP-0 and PP-4 as a function of draw ratio after drawing at 110°C. It is found that at lower draw ratios ($\lambda < 4$), addition of OMMT has little effect on the dichroic ratios of both the crystalline and amorphous bands. In contrast, at higher draw ratios, R of the crystalline band in PP-0 is larger than R of the crystalline band in PP-4, and $1/R$ of the amorphous phase PP-0 is larger than $1/R$ of the amorphous band in PP-4. This indicates that OMMT layers can hinder the orientation of both the crystalline and amorphous phases at this draw temperature. The phenomenon that nanofillers with high aspect ratio could retard orientation of polymer crystals was also previously reported for polyethylene/OMMT and polyethylene/inorganic whisker nanocomposites.[37,38] One can also see from Figure 5 that the dichroic ratios of the crystalline phase are far larger than those of the amorphous phase in the same samples. Figure 6 shows R of the crystalline band at 841 cm^{-1} and $1/R$ of the amorphous band at 2725 cm^{-1} for PP-0 and PP-4 as a function of draw ratio after drawing at 138°C. For the orientation of the crystalline phase, the effect of OMMT is similar to that at the draw temperature of 110°C,

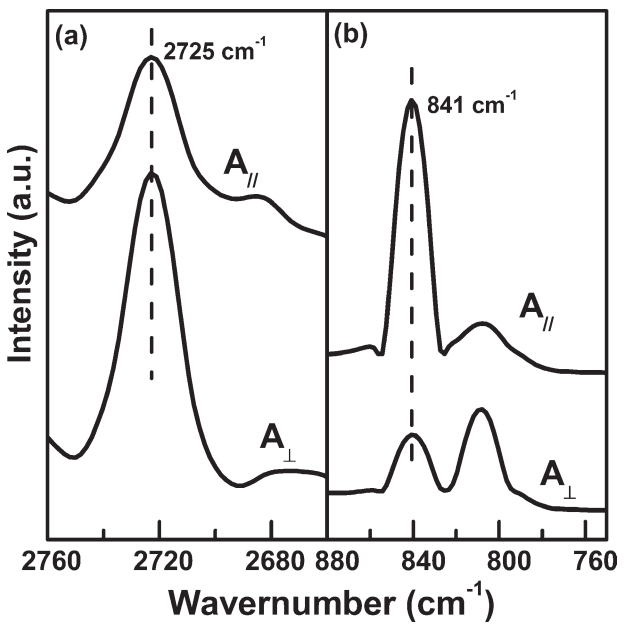

Figure 4 Polarized IR spectra with polarization vector parallel ($A_{||}$) and perpendicular ($A_{\perp}$) to the draw direction for neat PP (PP-0) after drawing at 138°C with λ = 3.5. (a) The amorphous band at 2725 cm^{-1}, (b) the crystalline band at 841 cm^{-1}.

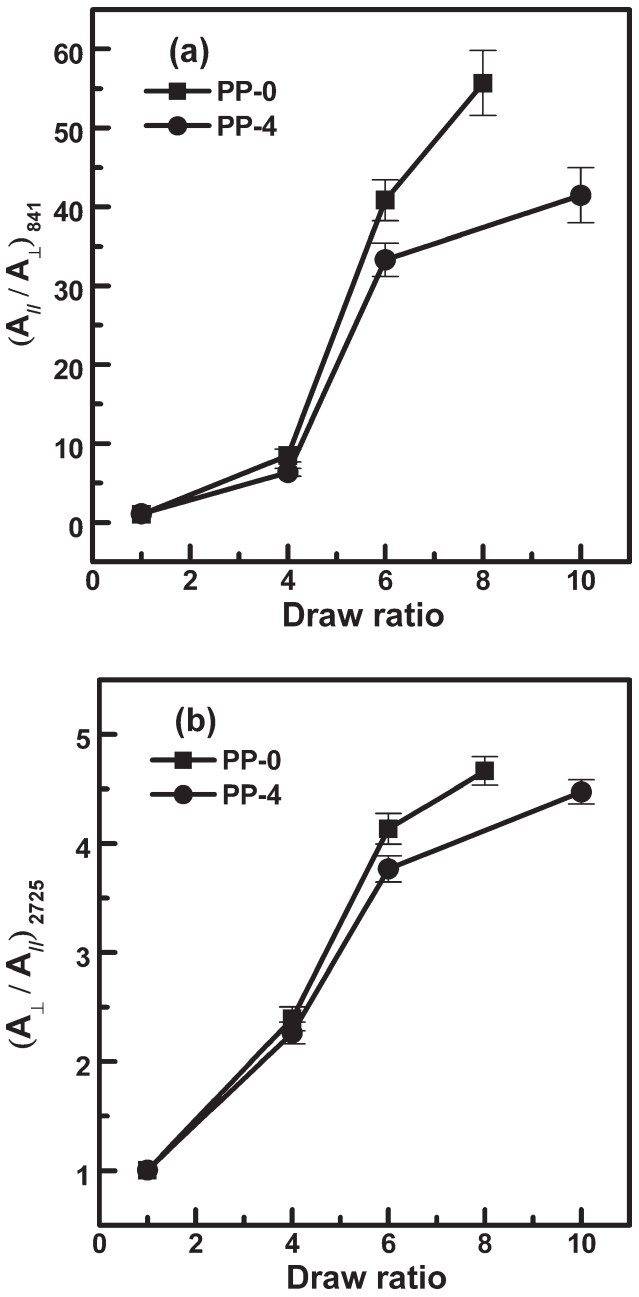

Figure 5 Dichroic ratios of the crystalline band at 841 cm^{-1} (a) and inversion of dichroic ratios of the amorphous band at 2725 cm^{-1} (b) for PP-0 and PP-4 as a function of draw ratio at a draw temperature of 110°C.

since the values of R for PP-4 are smaller than those for PP-0 at the same draw ratio. However, for the orientation of the amorphous phase, the effect of OMMT becomes reverse as compared with the result at draw temperature of 110°C. At higher draw ratios, $1/R$ of PP-4 is larger than that of PP-0. This shows that at higher draw ratios, OMMT layers hinder the orientation of the crystalline phase, but facilitate the orientation of the amorphous phase.

Figure 7 shows the dichroic ratios of the crystalline band at 841 cm^{-1} and inversion of dichroic ratios of the amorphous band at 2725 cm^{-1} as a function of OMMT loading at a draw temperature of 138°C and a draw ratio of 7. It is found that for the crystalline band, the dichroic ratio decreases monotonously as the OMMT content increases, indicating that the retardance effect of OMMT on orientation of the crystalline phase becomes more and more severe. On the other hand, one can see from Figure 7 that at lower OMMT loading ($\leq$4 wt %) the orientation degree of the amorphous phase increases with the OMMT content. However, when the OMMT

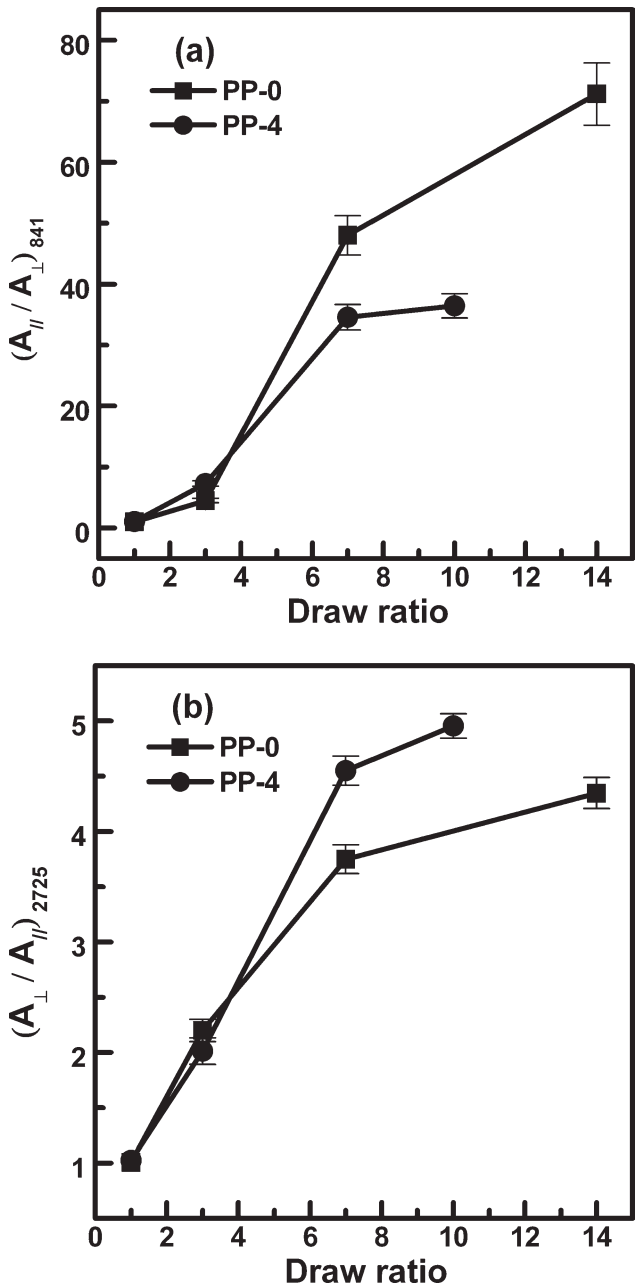

Figure 6 Dichroic ratios of the crystalline band at 841 cm^{-1} (a) and inversion of dichroic ratios of the amorphous band at 2725 cm^{-1} (b) for PP-0 and PP-4 as a function of draw ratio at a draw temperature of 138°C.

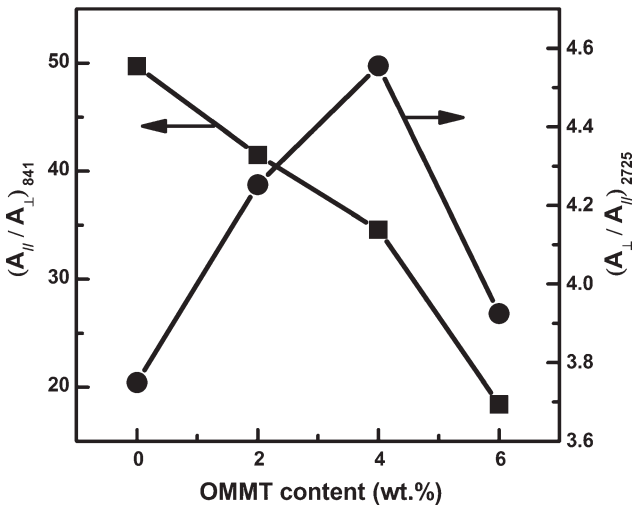

Figure 7 Dichroic ratios of the crystalline band at 841 cm^{-1} and inversion of dichroic ratios of the amorphous band at 2725 cm^{-1} as a function of OMMT loading at a draw temperature of 138°C and a $\lambda = 7$.

loading is beyond 4 wt %, the orientation degree of the amorphous phase falls down. This shows that at high draw temperature (138°C), addition of a small amount of OMMT in PP is advantageous to the orientation of the amorphous phase, but at high OMMT loading the retardance effect on orientation becomes evident, resulting in decreases of the orientation degree of the amorphous phase.

The polarized IR results show that the montmorillonite layers retard the orientation of the crystalline phase at both low and high temperatures. This observation is different from result obtained by shearing the nanocomposite melt. Many authors observed that shearing of polymer/montmorillonite nanocomposite melt can enhance the orientation of polymer crystals, as compared with shearing the neat polymer melt.[24,30] On the other hand, OMMT layers hinder the orientation of the amorphous phase at low draw temperature, but facilitate its orientation at high draw temperature and low OMMT loading. In both cases, temperature plays a key role. As a result, we try to interpret the effect of OMMT on orientation of the crystalline and amorphous

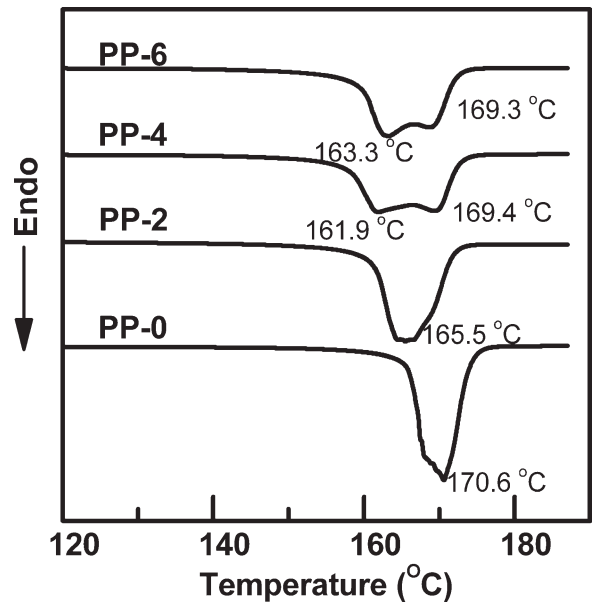

Figure 8 DSC melting traces of the drawn PP and PP/OMMT films. The films were drawn at 138°C with a $\lambda = 7$ and the heating rate was 10°C/min.

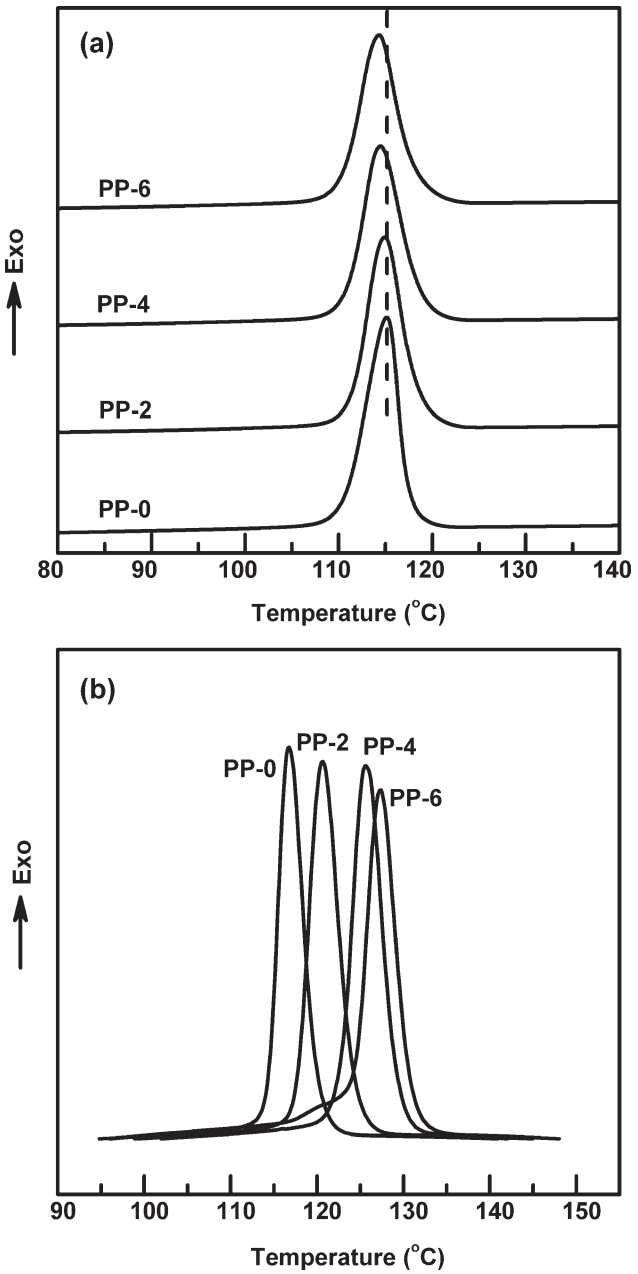

Figure 9 Nonisothermal crystallization DSC curves after the drawn PP and PP/OMMT films were held at 230°C (a) or 180°C (b) for 5 min and then cooled to room temperature at a rate of 10°C/min. The films were drawn at 138°C with a $\lambda = 7$.

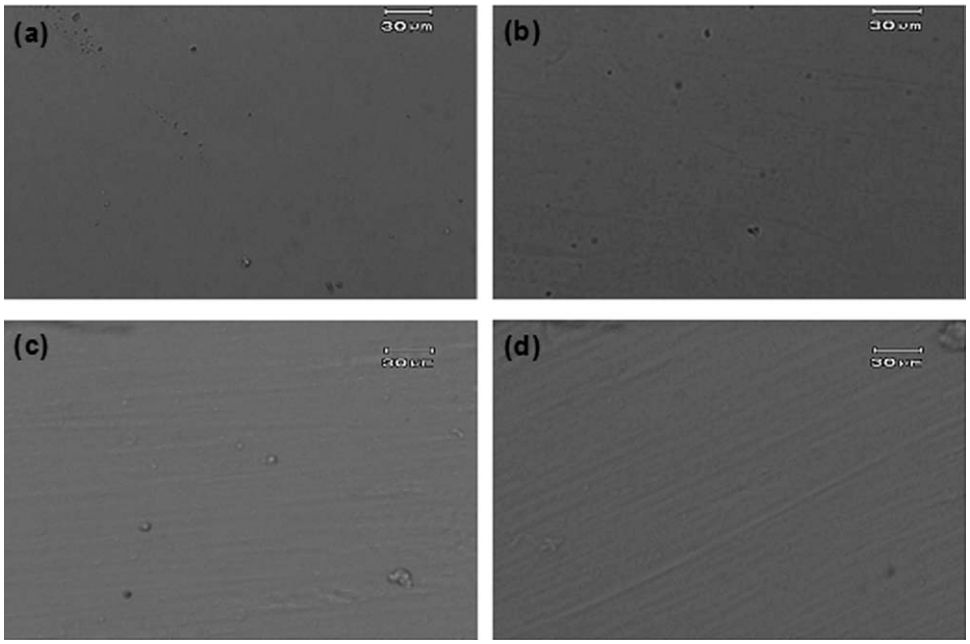

Figure 10 POM micrographs of the drawn PP and PP/OMMT films at 180°C for PP-0 (a), PP-2 (b), PP-4 (c), and PP-6 (d).

phases at different temperatures in terms of mobility of the two phases. The mobility of polymer crystals phase is very low before melting because of the ordered structure. Upon tensile drawing, the crystals may deform and reorganize. As a result, OMMT layers, which are platelets of large size, hinder the reorganization and orientation of the polymer crystals anyway, irrespective of the draw temperature. However, for the disordered amorphous phase, the mobility of the amorphous polymer chains is strongly dependent on temperature. At low temperature, the mobility of the amorphous phase is still lower, thus its orientation is hindered by OMMT layers. In contrast, at high temperature, the mobility of the amorphous is quite high, which means that the relaxation of the polymer chains in the amorphous phase is fast and even the relaxation rate of the amorphous PP chains may prevail against their orientation rate. When the amorphous phase orientates due to tensile drawing at high temperature, it is also easy to relax back to the unorientated state. The presence of OMMT layers can stabilize the stretched conformation and prevent the orientated polymer chains from relaxation, as we reported in electrospinning of PVDF/OMMT nanocomposites,[46] leading to the favorable effect of OMMT on orientation. When polymer crystals are melted, the polymer chains also become amorphous. Since melting of polymer crystals occurs at higher temperature, the stabilization effect of the OMMT layers becomes obvious. This is the reason why shearing polymer/montmorillonite nanocomposite melt leads to higher orientation degree than shearing the neat polymer melt. Moreover, when the OMMT loading is high, intercalated structure becomes the majority, as can be seen from Figures 2(c) and 3. When polymer chains are intercalated into the galleries of OMMT layers, the mobility of polymer chains is greatly reduced.[11–14] This means that increase of OMMT content is equivalent to decrease of draw temperature. As a result, at 6% OMMT loading, the OMMT layers retard the orientation of the amorphous phase even at the draw temperature of 138°C.

DSC result

To verify the stabilization effect of OMMT on the conformation of the amorphous phase, the melting and crystallization behaviors of the drawn films were characterized by DSC and morphologies of the drawn PP/OMMT films after melting and recrystallization were observed with POM. Figure 8 shows the DSC melting curves of the drawn films. The films were first drawn at 138°C with a $\lambda = 7$ prior to DSC characterization. It is observed that PP-0 nearly exhibits single melting peak with a melting temperature of 170.6°C, while PP-2 shows a broad melting peak with the peak temperature located at 165.5°C. Double melting peaks can clearly be seen from Figure 8 for the other two drawn samples PP-4 and PP-6. The low temperature peaks of PP-4 and PP-6 are located at 161.9 and 163.3°C, respectively, and the positions of the high temperature peaks are similar to that of PP-0. The melting behaviors of the drawn films show that imperfect crystals are formed in the samples with high OMMT content. This is in

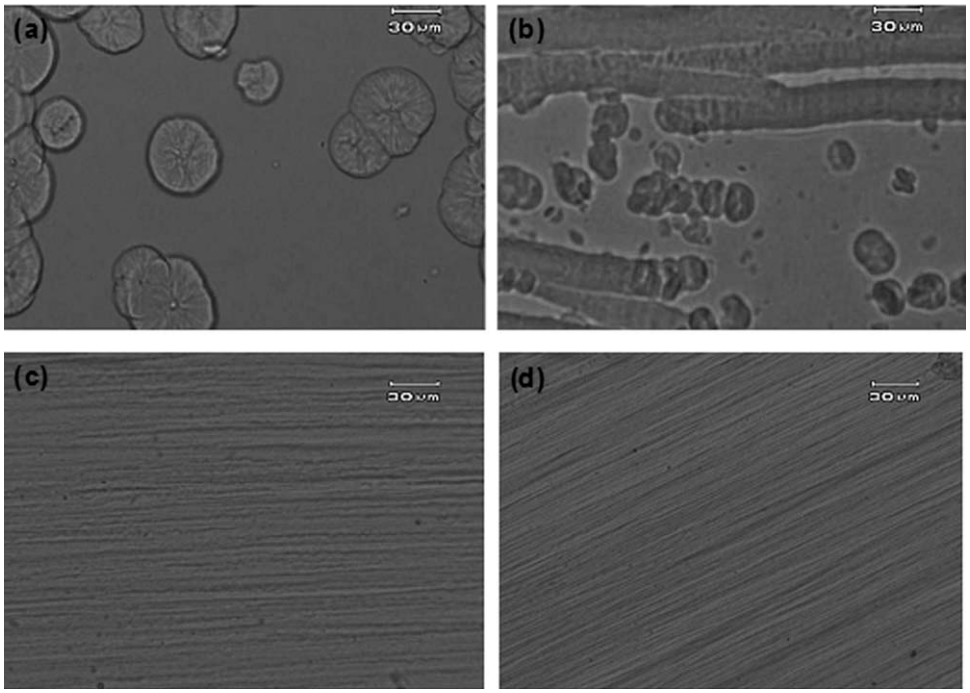

Figure 11 POM micrographs of PP and PP/OMMT during recrystallization after the drawn films were held at 180°C for 5 min and then cooled to room temperature at a rate of 2°C/min. The films were drawn at 138°C with a $\lambda = 7$. (a) PP-0 at 130°C, (b) PP-2 at 134°C, (c) PP-4 at 145°C, (d) PP-6 at 140°C.

accordance with the IR result that OMMT layers hinder the orientation of the crystalline phase. The nonisothermal crystallization DSC curves were also recorded after the drawn films were held at 180 or 230°C for 5 min (Fig. 9). As shown in Figure 9(a), when the drawn films were cooled from 230°C, all the four samples have similar crystallization temperatures. The crystallization temperatures of the samples PP-4 and PP-6 are even slightly lower than that of PP-0. No nucleation effect of the OMMT filler, which usually increases the crystallization temperature of semicrystalline polymers, is observed in such a situation. This is probably due to the presence of the PP-*g*-MA compatibilizer, which may weaken the nucleation effect of the OMMT layers. The melting curves show that all the drawn films are completely melted at 180°C. Therefore, the drawn films were also held at 180°C for 5 min and then cooled to room temperature. The recorded nonisothermal crystallization DSC curves were illustrated in Figure 9(b). One can see from Figure 9(b) that in this case the crystallization temperature increases gradually with the OMMT content in the samples. The sample PP-0 exhibits similar crystallization temperatures when cooled from 180 and 230°C, but for the other three samples containing OMMT the crystallization

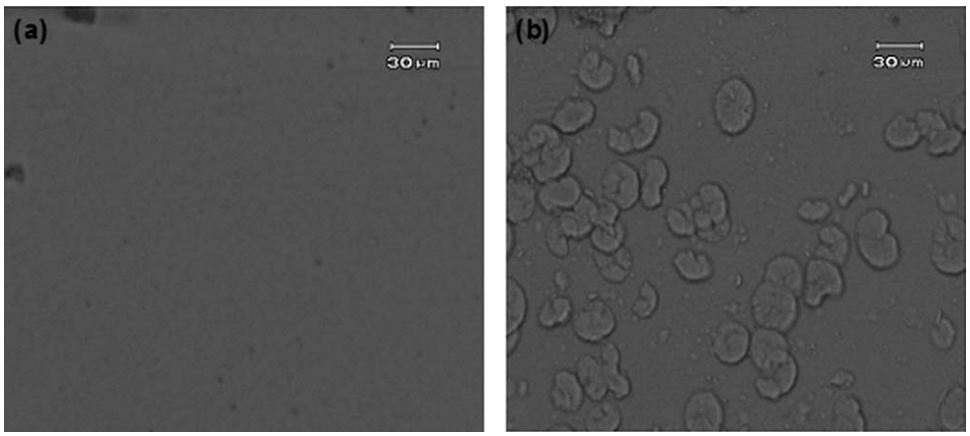

Figure 12 POM micrographs of drawn PP-4 film at 230°C (a) and during recrystallization cooled from 230°C at a rate of 2°C/min (b). The PP-4 film was drawn at 138°C with a $\lambda = 7$.

temperature is higher when cooled from 180°C. Since the nucleation effect of OMMT is absent, which is revealed by the nonisothermal crystallization DSC curves cooled from 230°C, the increase of crystallization temperature with OMMT content for the drawn films cooled from 180°C can be attributed to so-called "memory effect." The memory effect, which means that the conformation of polymer in the melts can affect its crystallization behavior, is widely observed in crystallization of PP and other semicrystalline polymers.[47–57] It is found that, when the neat PP films are cooled from 180°C and 230°C, respectively, the crystallization temperatures are similar, which are 116°C and 117°C. This shows that the memory effect is not evident for the neat PP film. In contrast, the drawn PP/OMMT films cooled from 180°C always exhibit higher crystallization temperature than the corresponding samples cooled from 230°C. Therefore, OMMT layers can intensify the memory effect. The intensification of the memory effect by OMMT further supports the conclusion that OMMT layers can stabilize the amorphous conformation with a fast relaxation rate at high temperature. The similar crystallization for the drawn films cooled from 230°C also shows that such a stabilization effect disappears due to the fast relaxation rate at this temperature.

POM observations

Figure 10 shows the POM micrographs of the drawn PP and PP/OMMT films at 180°C. For the neat PP and PP-2, the images are basically featureless because all the crystals are melted. In contrast, for PP-4 and PP-6, fibril texture is observed though the samples are in the molten state and the fibril structure is more obvious in PP-6. After the drawn films were held at 180°C for 5 min, the melted films were then cooled to room temperature at a rate of 2°C/min for recrystallization and the morphology during cooling was recorded (Fig. 11). It is found that spherulites are formed for the drawn film of neat PP without OMMT. For the drawn PP-2 film, orientated cylindrites of spherulite together with scattered spherulites are observed. In the drawn PP-4 film, the scattered spherulites disappear and only orientated cylindrites are observed. Moreover, the transverse size of the cylindrites in the drawn PP-4 film is much smaller than that in PP-2. In the drawn PP-6 film, the transverse size of the cylindrites becomes so small that only fibril crystals are observed. Figure 11 clearly reveals that the conformation of PP can be preserved to some extent by OMMT layers, though PP chains are melted.

It should be noted that the stabilization effect of the OMMT layer is limited and depends on temperature. For example, when the drawn film of PP-4 was held at 230°C for 5 min and then cooled to room temperature at a rate of 2°C/min, we find that the fibril texture disappears [Fig. 12(a)], which is in contrast with the morphology at 180°C [Fig. 10(c)]. After PP-4 is cooled from 230°C to room temperature for recrystallization, only spherulites are formed [Fig. 12(b)] and no orientated cylindrites are observed [Fig. 11(c)]. This shows that the stabilization effect of the OMMT layer on the conformation of amorphous chains disappears at 230°C.

CONCLUSIONS

Above results show that the effects of OMMT layers on the orientations of the crystalline and amorphous phases are determined by the competition of the polymer chain mobility (related to temperature and OMMT loading) and stabilization effect of OMMT layers. For the crystalline phase with a low mobility, OMMT layers hinder its orientation at both low and high draw temperatures. However, for the amorphous phase, the retardance effect on its orientation prevails at low draw temperature and/or at high OMMT loading. When the OMMT content is low and the draw temperature is high, the stabilization effect on the conformation of polymer chains plays the major role, leading to higher orientation degree of the amorphous phase. The stabilization effect of OMMT on the conformation of polymer chains are verified by the nonisothermal crystallization behavior of the drawn films and the morphology of the drawn PP/OMMT films after melting at 180°C and recrystallization.

References

1. Messersmith, P. B.; Giannelis, E. P. J Polym Sci Part A: Polym Chem 1995, 33, 1047.
2. Gopakumar, T. G.; Lee, J. A.; Kontopoulou, M.; Parent, J. S. Polymer 2002, 43, 5483.
3. Wang, K. H.; Choi, M. H.; Koo, C. M.; Xu, M. Z.; Chung, I. J.; Jang, M. C.; Choi, S. W.; Song, H. H. J Polym Sci Part B: Polym Phys 2002, 40, 1454.
4. Ray, S. S.; Okamoto, M. Macromol Rapid Commun 2003, 24, 815.
5. Jiang, T.; Wang, Y. H.; Yeh, J. T.; Fan, Z. Q. Eur Polym J 2005, 41, 459.
6. Shah, R. K.; Krishnaswamy, R. K.; Takahashi, S.; Paul, D. R. Polymer 2006, 47, 6187.
7. Ma, J. S.; Zhang, S. M.; Qi, Z. N.; Li, G.; Hu, Y. L. J Appl Polym Sci 1978, 2002, 83.
8. Zhang, Q. X.; Yu, Z. Z.; Yang, M. S.; Ma, J.; Mai, Y. W. J Polym Sci Part B: Polym Phys 2003, 41, 2861.
9. Nam, J. Y.; Ray, S. S.; Okamoto, M. Macromolecules 2003, 36, 7126.
10. Rozanski, A.; Monasse, B.; Szkudlarek, E.; Pawlak, A.; Piorkowska, E.; Galeski, A.; Haudin, J. M. Eur Polym J 2009, 45, 88.
11. Somwangthanaroj, A.; Lee, E. C.; Solomon, M. J. Macromolecules 2003, 36, 2333.
12. Di Maio, E.; Iannace, S.; Sorrentino, L.; Nicolais, L. Polymer 2004, 45, 8893.

13. Xu, J. T.; Wang, Q.; Fan, Z. Q. Eur Polym J 2005, 41, 3011.
14. Xu, J. T.; Zhao, Y. Q.; Wang, Q.; Fan, Z. Q. Macromol Rapid Commun 2005, 26, 620.
15. Zhang, Q.; Wang, Y.; Fu, Q. J Polym Sci Part B: Polym Phys 2003, 41, 1.
16. Zhang, X. Q.; Yang, M. S.; Zhao, Y.; Zhang, S. M.; Dong, X.; Liu, X. X.; Wang, D. J.; Xu, D. F. J Appl Polym Sci 2004, 92, 552.
17. Joshi, M.; Shaw, A.; Butola, B. S. Fiber Polym 2004, 5, 59.
18. Joshi, M.; Viswanathan, V. J Appl Polym Sci 2006, 102, 2164.
19. Lee, S. H.; Youn, J. R. J Appl Polym Sci 2008, 109, 1221.
20. Koo, C. M.; Kim, J. H.; Wang, K. H.; Chung, I. J. J Polym Sci Part B: Polym Phys 2005, 43, 158.
21. Wang, K.; Liang, S.; Zhang, Q.; Du, R. N.; Fu, Q. J Polym Sci Part B: Polym Phys 2005, 43, 2005.
22. Sun, T. C.; Chen, F. H.; Dong, X.; Zhou, Y.; Wang, D. J.; Han, C. C. Polymer 2009, 50, 2465.
23. Kim, K. J.; Lee, J. S.; Prabu, A. A.; Kim, T. H. Polym Compos 2009, 30, 265.
24. Wang, K.; Xiao, Y.; Na, B.; Tan, H.; Zhang, Q.; Fu, Q. Polymer 2005, 46, 9022.
25. Kim, G. M.; Lee, D. H.; Hoffmann, B.; Kressler, J.; Stoppelmann, G. Polymer 2001, 42, 1095.
26. Maiti, P.; Okamoto, M. Macromol Mater Eng 2003, 288, 440.
27. Wan, T.; Chen, L.; Chua, Y. C.; Lu, X. H. J Appl Polym Sci 2004, 94, 1381.
28. Nowacki, R.; Monasse, B.; Piorkowska, E.; Galeski, A.; Haudin, J. M. Polymer 2004, 45, 4877.
29. Mago, G.; Fisher, F. T.; Kalyon, D. M. Macromolecules 2008, 41, 8103.
30. Yalcin, B.; Valladares, D.; Cakmak, M. Polymer 2003, 44, 6913.
31. Park, S. Y.; Cho, Y. H. Macromol Res 2005, 13, 156.
32. Park, S. Y.; Cho, Y. H.; Vaia, R. A. Macromolecules 2005, 38, 1729.
33. Ibanes, C.; de Boissieu, M.; David, L.; Seguela, R. Polymer 2006, 47, 5071.
34. Xu, B.; Leisen, J.; Beckham, H. W.; Abu-Zurayk, R.; Harkin-Jones, E.; McNally, T. Macromolecules 2009, 42, 8959.
35. Khan, A. N.; Hong, P. D.; Chuang, W. T.; Shih, K. S. Polymer 2009, 50, 6287.
36. Rajeev, R. S.; Harkin-Jones, E.; Soon, K.; McNally, T.; Menary, G.; Armstrong, C. G.; Martin, P. J. Eur Polym J 2009, 45, 332.
37. Wang, K. H.; Chung, I. J.; Jang, M. C.; Keum, J. K.; Song, H. H. Macromolecules 2002, 35, 5529.
38. Su, R.; Wang, K.; Ning, N. Y.; Chen, F.; Zhang, Q.; Wang, C. Y.; Fu, Q.; Na, B. Compos Sci Technol 2010, 70, 685.
39. Song, Y. H.; Nitta, K. H.; Nemoto, N. Macromolecules 2003, 36, 8066.
40. Song, Y. H.; Nitta, K. H.; Nemoto, N. Macromolecules 2003, 36, 1955.
41. Carretero-Gonzalez, J.; Verdejo, R.; Toki, S.; Hsiao, B. S.; Giannelis, E. P.; Lopez-Manchado, M. A. Macromolecules 2008, 41, 2295.
42. Toki, S.; Hsiao, B. S. In Advanced Structured Materials; Mittal, V.; Kim, J. K.; Pal, K., Eds.; Springer:Heidelberg, 2011, p 135.
43. Mirabella, F. M. J Polym Sci Part B: Polym Phys 1987, 25, 591.
44. Karacan, I.; Taraiya, A. K.; Bower, D. I.; Ward, I. M. Polymer 1993, 34, 2691.
45. Schmidt, P.; Raab, M.; Kolarik, J.; Eichhorn, K. J. Polym Test 2000, 19, 205.
46. Liu, Y. L.; Li, Y.; Xu, J. T.; Fan, Z. Q. ACS Appl Mater Interfaces 2010, 2, 1759.
47. Huang, L. Q.; Pan, L. H.; Inoue, T. J Appl Polym Sci 2007, 104, 787.
48. Lorenzo, A. T.; Arnal, M. L.; Sanchez, J. J.; Muller, A. J. J Polym Sci Part B: Polym Phys 2006, 44, 1738.
49. Hafele, A.; Heck, B.; Hippler, T.; Kawai, T.; Kohn, P.; Strobl, G. Eur Phys J E Soft Matter 2005, 16, 217.
50. Supaphol, P.; Srimoaon, P.; Sirivat, A. Polym Int 2004, 53, 1118.
51. Sisti, L.; Finelli, L.; Lotti, N.; Berti, C.; Munad, A. E-Polymers 2003.
52. D'Ilario, L.; Martinelli, A.; Piozzi, A. J. Macromol Sci Phys 2002, B41, 47.
53. Zhu, X. Y.; Yan, D. Y. Colloid Polym Sci 2001, 279, 546.
54. Zhu, X. Y.; Li, Y. J.; Yan, D. Y.; Fang, Y. P. Polymer 2001, 42, 9217.
55. Zhu, X. Y.; Yan, D. Y.; Yao, H. X.; Zhu, P. F. Macromol Rapid Commun 2000, 21, 354.
56. Alfonso, G. C.; Scardigli, P. Macromol Symp 1997, 118, 323.
57. Alfonso, G. C.; Ziabicki, A. Colloid Polym Sci 1995, 273, 317.